Dynamics in the metabasin space of a Lennard-Jones glass former: Connectivity and transition rates

Yasheng Yang and Bulbul Chakraborty

Martin Fisher School of Physics, Brandeis University, Mailstop 057, Waltham, Massachusetts 02454-9110, USA

Using simulations, we construct the effective dynamics in metabasin space for a Lennard-Jones glass former. Metabasins are identified via a scheme that measures transition rates between inherent structures and generates clusters of inherent structures by drawing in branches that have the largest transition rates. This construction is fundamentally different from the stochastic approach based on molecular-dynamics trajectories. The effective dynamics in this metabasin space is shown to be Markovian but to differ significantly from the simplest trap models. We specifically show that retaining information about the connectivity in this metabasin space is crucial for reproducing the slow dynamics observed in this system.

I. INTRODUCTION

The origin of the dramatic slowing down of dynamics in supercooled liquids upon approaching the glass transition temperature has been of great research interest. The potential-energy landscape (PEL) has proved to be an important conceptual tool for analyzing the dynamics of supercooled liquid [1–6]. In PEL picture, the configuration hyperspace can be separated into a collection of potential-energy valleys, each identified with a local minimum or "inherent structure (IS)." There have been many recent studies demonstrating that the low-temperature dynamics of model supercooled liquids is dominated by activated dynamics between "traps" represented by metabasins which are clusters of inherent structures [7–9]. In this activated regime, a natural mechanism for glassy dynamics is provided by the trap model [10]. Extensive numerical simulations of model glass formers have shown that the dynamics in metabasin space can be mapped on to the original [11] or an extended version of the trap model [12]. The trap model framework neglects the connectivity in the metabasin space. Since metabasins are necessarily defined through some dynamic criteria, it can be expected that the connectivity in this space depends on the method of construction. An interesting question to ask is whether a nontrivial connectivity in a metabasin space, such as the one found in the multiple funnel landscape [13,14], leads to important differences from the trap model predictions regarding diffusion constants and relaxation time scales.

An important ingredient in any framework for mapping the dynamics of a supercooled liquid to metabasin space is the method for constructing the metabasin. In previous work, metabasins were extracted from molecular-dynamics trajectories projected on to the inherent-structure space [12], where it was observed that there were long stretches where the system transitioned back and forth between a finite number of inherent structures, and these were grouped into metabasins. The usefulness of the metabasin concept lies in the enormous simplification in the dynamics that results from projecting the supercooled-liquid dynamics on to the metabasin space: this projected dynamics is [12], and therefore,

understanding glassy dynamics reduces to the problem of understanding the properties of this random walk. Adopting the perspective that the aim of the metabasin construction is to define a space in which the complex dynamics of the supercooled liquid becomes Markovian, opens up the possibility of constructing metabasins using other algorithms. In this paper, we pursue this line of reasoning and use a metabasin construction scheme based on a knowledge of the transition rates between different inherent structures. With the metabasins defined, we (a) test whether a trap model with these metabasins as the traps provides an adequate description of the observed dynamics of the supercooled liquid, (b) include the connectivity in the metabasin space to extend the trap model predictions and show that the correlations extracted from this random walk, which takes into account the nontrivial connectivity, agrees well with the ones measured directly in the molecular-dynamics simulations, and finally (c) we analyze the properties of this random walk in order to gain some insight into the slow dynamics.

II. MODEL

The model system we use to study the dynamics of supercooled liquid is a Lennard-Jones binary mixture consisting of 67 particles: 53 of type A and 14 of type B. To study dynamics in configuration space, it is essential to focus on small systems since many features get washed out for larger systems [4]. The simulation box used in our study is a cube with periodical boundary condition. All particles have the same mass m, and they interact via a Lennard-Jones potential $v(r) = 4\epsilon[(\sigma/r)^{12} - (\sigma/r)^6]$, where r is the distance between them. The interaction parameters, depending on the types of participating particles, are $\epsilon_{AA} = 1.0$, $\sigma_{AA} = 1.0$, $\epsilon_{AB} = 1.5$, $\sigma_{AB} = 0.8$, $\epsilon_{BB} = 0.5$, and $\sigma_{BB} = 0.88$ [15]. In the following, all quantities will be expressed in reduced units, with the unit of length as σ_{AA}, the unit of energy as ϵ_{AA}, and the unit of time as $(m\sigma_{AA}^2/\epsilon_{AA})^{1/2}$ [16]. The number density of particles is 1.2. To accommodate the box with periodic boundary conditions, the potential is shifted and truncated with a quadratic cutoff [16–19], which ensures continuity of the potential and its gradient at the cut-off radius.

The modified potential is

$$v^c(r) = v(r) - v(r_c) - \frac{(r^2 - r_c^2)}{2 r_c}\left(\frac{dv(r)}{dr}\right)_{r=r_c}$$

$$= 4\epsilon\{(\sigma/r)^{12} - (\sigma/r)^6 + [6(\sigma/r_c)^{12} - 3(\sigma/r_c)^6](r/r_c)^2$$

$$- 7(\sigma/r_c)^{12} + 4(\sigma/r_c)^6\}, \tag{1}$$

for $r < r_c$ and $v^c(r) = 0$ for $r \geq r_c$. Since the cut-off distance should be smaller than half of the box size, a cut-off distance $r_c = 1.9$ is used. This cutoff makes the potential shallower than the original [15], and, therefore, the ratio between A and B particles is adjusted to minimize the chances of crystallization. The velocity form of Verlet algorithm is used to solve the Newtonian equation, with $\delta t = 0.001$. Temperature is fixed by resampling the velocities from a Boltzmann distribution after every 10240 simulation steps. Initial configurations are generated by first equilibrating the system at $T = 5$, then at $T = 2$, and then slowly cooling down to the temperatures of interest with cooling rate $\leq 3.33 \times 10^{-6}$ [20] (smaller cooling rates are used at lower temperatures). At each of these temperatures, the system is equilibrated for a time much longer than (at least an order of magnitude) the estimated α-relaxation time before any data is collected for measurement.

The temperature range considered is from $T = 0.7$ to $T = 0.48$. For the truncated shallower potential used in this work, over this temperature range, the supercooled liquid slows down significantly with values of the α-relaxation time approaching 10^3, yet its equilibrium properties can be studied in simulations. Studies using a potential very similar to the one employed here (differing only in the cut-off length) have shown that finite-size effects are negligible in 65-particle systems [8,12]. Specifically, it has been shown that the diffusion constant obtained from a system of this size is identical to that of a 1000 particle system [8], and it has also been shown that it is possible to obtain information about lengths scales of dynamical heterogeneities in the context of an extended trap model for a 65-particle system [12]. Size of the cooperatively rearranging region during a metabasin transition can indeed be larger than that involved in a dynamical heterogeneity [21]. In the discussion section, we address specific finite-size issues in the context of the conclusions reached in this paper.

III. INHERENT STRUCTURES

ISs are obtained using conjugate gradient minimization techniques during the simulation [3,6]. Although, theoretically, inherent structures can be labeled by their exact potential energy, there is a danger of labeling two different inherent structures with the same potential energy since any numerical procedures measure the potential energy with finite precision. To alleviate this problem, we use a pair of energies to label each inherent structure $\{V, V_{BB}\}$, where V is the potential energy of local minima and V_{BB} is the potential energy between type B particles. If two different inherent structures have the same V, their V_{BB} are likely to be different since they have different arrangement of particles. Imple-
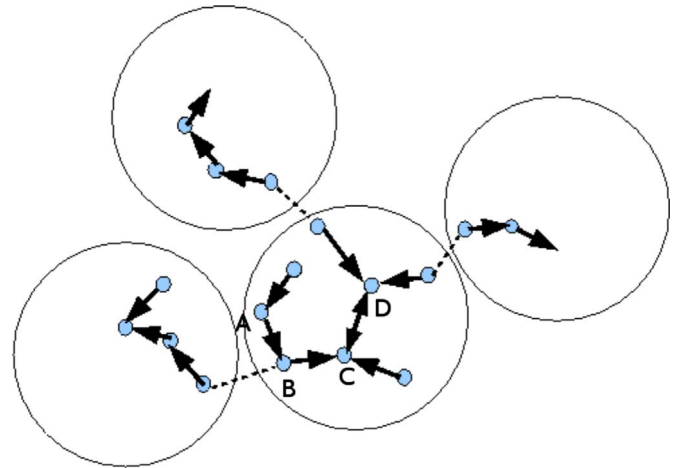

FIG. 1. (Color online) Illustration of the construction of metabasins. Small circles denote inherent structures. Solid arrows denote the strongest transition branches from corresponding metabasins. Each big circle encloses a cluster of inherent structures, i.e., a metabasin. Dash lines denote the weaker intermetabasin transitions.

menting this procedure is most important for the metabasin construction since many thousands of IS are generated in the process.

Given an inherent structure, an ensemble of configurations in the same valley can be constructed by using a restricted Boltzmann sampling that is discussed in the next section. With each of these configurations and initial velocities sampled from the Boltzmann distribution, the waiting time out of this IS valley can be measured using the interval-bisection method [9]. For the temperature range considered in this paper, it turns out that for many inherent structures, the distribution of waiting time deviates from exponential significantly; thus, the transition between inherent structures is history dependent. The history dependence indicates that there is no clear separation of scales between the time taken to equilibrate in an IS valley and the hopping between different IS. This is reasonable given the fact that there can be arbitrarily small dynamical barriers between the IS, which are defined solely based on their property of being a potential-energy minimum. It is expected that grouping IS into metabasins such that IS with frequent transitions between them are in the same metabasin would lead to larger barriers between metabasins, and, therefore, a separation of time scales and Markovian dynamics.

IV. CONSTRUCTION OF METABASINS

Starting from one inherent structure in a hypothetical metabasin, the system will more likely go into another inherent structure in the same metabasin. To construct a metabasin from a randomly chosen inherent structure A, we—therefore—need to start the simulation from A for many times and count how many times the system goes into each neighboring inherent structure. There must be a most frequently visited neighbor B. Or in other words, A has stronger connection to B than to any of its other neighbors. As shown in Fig. 1, A and B get connected by an arrow. The procedure

is repeated starting with *B* and the process of building this cluster continues until we find a connection, which links two ISs that are already in the cluster. All the IS in the cluster are now assigned to one metabasin. We then check the other neighboring IS found in the process of constructing the cluster and identify their most frequently visited neighbor. If these belong to the existing cluster then these ISs also get assigned to the metabasin containing the starting configuration *A*. During the construction of metabasin, tens of thousands of inherent structures are encountered, which crowd into a small range of potential energy, and as mentioned earlier, it becomes essential to label them with both $\{V, V_{BB}\}$.

Our construction is similar to the hierarchical master-equation approach in [22]. Comparing with metabasin (MB) construction methods based on trajectories, our approach is objective except for the fact that the computational force is limited to explore all the details of a MB in the phase space.

The construction of the metabasin described above relies on the transitions between IS being history independent. It is, therefore, important to obtain an initial *ensemble* of states which are in equilibrium in the valley *A* and use these as starting configurations to measure the number of transitions to other IS. All of these starting configurations should have the same set of values for $\{V, V_{BB}\}$ but a different set of velocities. We implement this restricted Boltzmann sampling by starting from an initial configuration A_0, with initial velocities sampled from the Boltzmann distribution and run the simulation for *n* molecular dynamics (MD) steps. If the final state A_1 still belongs to the same inherent structure then we accept it as a member of the ensemble. If not, we count A_0 again as a member of the ensemble. This process is repeated until we have a large enough ensemble of initial states to measure the transitions from. In practice, *n* is chosen to be 1/4 of the estimated waiting time of the given IS and, in order to reduce correlation, the above process is repeated eight times before the resulting state is accepted as initial state. The number of initial states is at least 40 and more often chosen to be greater for better estimation of branching ratios.

The temperature chosen to construct metabasin is *T* =0.52, a temperature where IS are well defined and the dynamics is not prohibitively slow for metabasin construction. The number of initial inherent structures randomly chosen from MD trajectories is 140 and each of these constitutes the starting point for metabasin construction according to the algorithm described above.

The potential energy *E* of a metabasin is defined to be the energy of the most probable inherent structure in it.

V. MARKOVIAN PROPERTY

A hallmark of Markovian processes is that the distribution of waiting times is exponential [23]. Since the motivation behind the construction of the metabasins is obtaining a Markovian model of the dynamics of supercooled liquids, the first task is to check whether our metabasin construction yields a space in which the dynamics is Markovian. To measure the waiting times, an ensemble of initial states is constructed through a restricted Boltzmann sampling in each
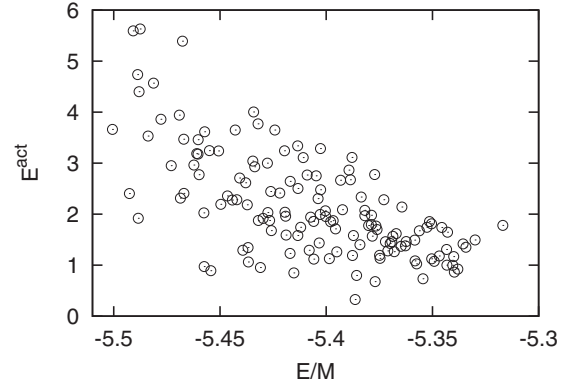

FIG. 2. Effective activation energy E^{act} of metabasins plotted against their energy per particle E/M, where *M* is the number of particles. The activation energies are calculated according to Eq. (2).

metabasin and at the temperature of interest. A constant-temperature trajectory is then started from each initial state, and the interval-bisection method [9] is used to determine the inherent-structure sequence of the trajectory. If the inherent structures of two successive quenches are not in the original metabasin, the system is considered to have made a transition to a new metabasin, and the waiting time is recorded. Since the conjugate gradient method used to minimize the potential energy occasionally leads to a wrong inherent structure, two successive quenches are used to signal a transition. For all the metabasins constructed according to our algorithm, the waiting time distributions are founded to be exponential and, therefore, the dynamics in this space is indeed Markovian. The mean waiting time τ_i for a metabasin *i* with energy E_i is measured in the temperature range $0.44 \leq T \leq 0.70$. This mean waiting time is found to be above the ballistic time region, indicating the separation of time scales that we would like to see for metabasins. The mean waiting time is characteristic of an activated process with

$$\tau_i(T) \approx \tau_i^{\infty} \exp(E_i^{act}/T). \tag{2}$$

The effective activation energy E^{act} is not strongly correlated with the energy *E* although E^{act} tends to be higher for lower lying metabasins, as shown in Fig. 2. The time scale $\tau(T)$ demonstrates a stronger correlation with a marked increase for deeper metabasins, as shown in Fig. 3. Since the dynamics in metabasin space is Markovian, the evolution of the probability distribution of metabasins $P_i(t)$ is described by

$$\frac{d}{dt} P_i(t) = -\frac{1}{\tau_i(T)} P_i(t) + \sum_j w_{ij} P_j(t), \tag{3}$$

where τ_i is the mean waiting time of metabasin *i* at temperature *T*, and w_{ij} is the transition rate from metabasin *j* to metabasin *i*. Envisioning the metabasins as traps of depth E_i^{act}, the simplest trap model is one that ignores the connectivity and characterizes the trap space by τ_i and a density of states [10],
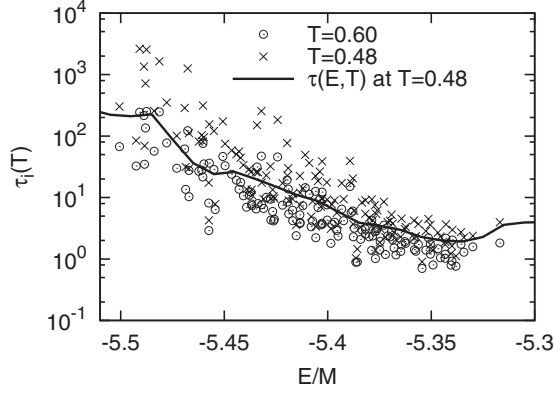
FIG. 3. Waiting time of metabasins measured at $T=0.6$ and 0.48 plotted against their metabasin energy per particle. The solid line is $\tau(E,T)$ calculated according to Eq. (6).

$$\frac{d}{dt}P_i(t) = -\frac{1}{\tau_i(T)}P_i(t) + \omega(t)\rho(E_i^{act}), \qquad (4)$$

where $\omega(t)$ is a normalization factor and $\rho(E^{act})$ is the density of traps with a depth E^{act}. In most mappings of metabasin dynamics, in Lennard-Jones systems, to trap models the energy of the metabasin, E has been considered as the depth of the trap. As discussed earlier, we find that the activation energy and the nominal energy of a metabasin are not strongly correlated. We, therefore, choose to construct an effective trap model that describes dynamics in an energy landscape, by averaging τ_i over metabasins with energies in a small range around a value E,

$$\frac{d}{dt}P(E,t) = -\frac{P(E,t)}{\tau(E,T)} + \rho(E,T)\omega(t), \qquad (5)$$

where

$$P(E,t) = \sum \delta(E_i - E)P_i(t),$$

$$\frac{1}{\tau(E,T)} = \frac{\sum\limits_{i} \delta(E_i - E)P_{i,eq}(T)/\tau_i(T)}{\sum\limits_{i} \delta(E_i - E)P_{i,eq}(T)},$$

$$\rho(E,T) = P_{eq}(E,T)/\tau(E,T),$$

$$\omega(t) = \frac{\sum\limits_{i} P_i(T)/\tau_i}{\sum\limits_{i} P_{i,eq}(T)/\tau_i}, \qquad (6)$$

with $P_{i,eq}(T) \propto \exp(-\beta E_i)$, the equilibrium probability of finding metabasin i, and $P_{eq}(E,T)$ as the equilibrium distribution of metabasin energy, which can be measured in the simulation. As shown below, this effective trap model differs from the simple trap model [10] in that $\rho(E,T)$ depends on temperature; reflecting the fact that E_i is not the trap depth of metabasin i.

The metabasin energy distribution $P_{eq}(E,T)$ is obtained from simulations run at $T=0.6$, 0.52, and 0.48 and is found to be well described by a Gaussian over this range
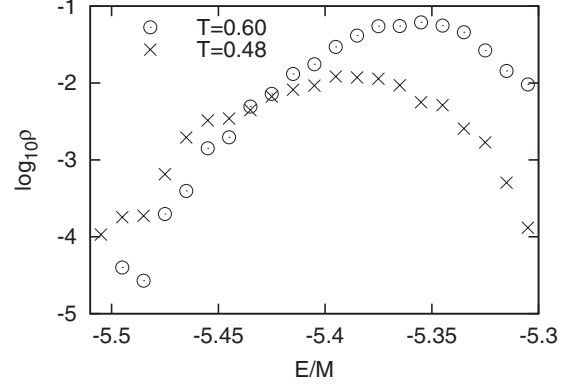

FIG. 4. Plot of the density of states of metabasins $\Omega(E)$ shifted vertically to make lines overlap.

[4,8,11,24]. We have extracted the density of states from these distribution and find that $\Omega(E) \propto P_{eq}(E,T)\exp(E/T)$ is, indeed, independent of temperature as shown in Fig. 4. We use this observation to construct $P_{eq}(E,T)$ at temperatures other than the ones where it was measured explicitly and combine this information with $\tau(E,T)$ to obtain $\rho(E,T)$. This function shown in Fig. 5 depends on temperature and is different from $\Omega(E)$.

The effective trap model based on the deduced forms of $\rho(E,T)$, $\tau(E,T)$, and $\omega(t)$ provides a description of the activated dynamics near the glass transition. It is, however, a mean-field model that ignores the connectivity in the metabasin space. In order to evaluate the effects of the connectivity on the dynamics, we have calculated various correlation functions using this trap model and compared it to the results of the direct molecular-dynamics simulations.

VI. TESTING THE TRAP MODEL

In this section, we compare the predictions of the effective trap model to actual simulation results. In the trap model, correlation functions are calculated by averaging over the sampled metabasins according to
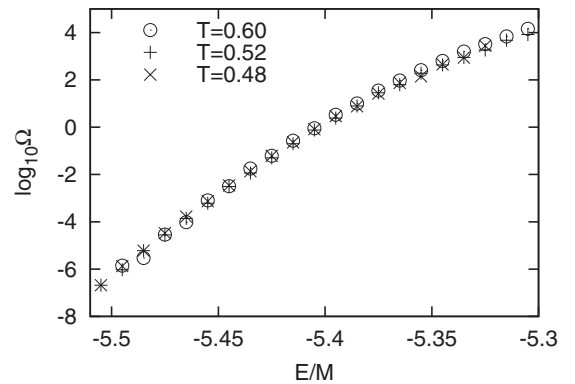

FIG. 5. $\rho(E,T)$ at $T=0.6$ and 0.48 calculated according to Eq. (6).

TABLE I. Comparison of estimates of the α relaxation time, τ_α, τ_s, and τ_c.

T	$\tau_\alpha(T)$	$\tau_s(T)$	$\tau_c(T)$	$\dfrac{\tau_\alpha(T)}{\tau_\alpha(0.6)}$	$\dfrac{\tau_s(T)}{\tau_s(0.6)}$	$\dfrac{\tau_c(T)}{\tau_c(0.6)}$
0.9	2.2	6.7		0.11	0.11	
0.6	20	62	2.9	1	1	1
0.52	91	2.7 × 10²	11	4.5	4.4	3.8
0.48	3.7 × 10²	1.1 × 10³	32	19	18	11
0.46	8.4 × 10²	2.5 × 10³		42	40	

$$\langle A \rangle_{eq} = \sum_i P_{i,eq}(T) A_i = \int dE\, P_{eq}(E,T)\, \frac{\sum\limits_i P_{i,eq}(T)\delta(E-E_i)A_i}{\sum\limits_i P_{i,eq}(T)\delta(E-E_i)}$$

$$= \int dE\, P_{eq}(E,T)\, \frac{\sum\limits_\alpha \delta(E-E_\alpha)A_\alpha}{\sum\limits_\alpha \delta(E-E_\alpha)}. \tag{7}$$

Here A is the physical observable of interest. The first summation Σ_i is over all metabasins, while Σ_α is over the metabasins, sampled according to the Boltzman distribution in the simulations. As mentioned earlier, a total of 140 metabasins was sampled. In numerical calculation, the δ function in Eq. (6) is replaced by a Gaussian with a narrow width $2\sigma^2 = 0.01^2 M^2$, with $M = 67$ being the number of particles.

A. Estimate of the alpha relaxation time

The α-relaxation time τ_α was measured in the simulation through its usual definition: $F_s(q_0, \tau_\alpha) = 1/e$, where $F_s(q,t)$ is the incoherent-scattering function [25]. In this paper, $F_s(q,t)$ is measured for type A particles and $q_0 = 7.251$ [15]. The α-relaxation time can also be estimated from the distribution of single-particle displacements [26], which shows marked non-Gaussianity at time scales on the order of τ_α. The non-Gaussianity is related to caging and a caging time scale τ_s can be extracted by measuring the time at which the probability of a type A particle having a translation less than $1/q_0$ diminishes to $1/e$. As shown in Table I, in the temperature range examined, τ_s and τ_α are proportional to each other. The caged motion of particles has also been related to hopping between metabasins [9].

In the trap model framework, the α-relaxation process corresponds to hopping between metabasins [9,11] and, in this regime, the correlation function $C(t)$ can be constructed by assuming that the correlation is unity when the system is in the same metbasin and drops to zero as it leaves the metabasin [10]. For our effective trap model, this approximation leads to

$$C(t) = \langle \exp(-t/\tau_i)\rangle_{eq}. \tag{8}$$

The expectation value is calculated according to Eq. (7). In Fig. 6, $C(t)$ is plotted along with $F_s(q,t)$. As expected, the shapes of the two functions are different since $C(t)$ has no information about the short-time dynamics. For $C(t)$ to be a useful tool for understanding the glass transition, however, the change in time scale of the long-time dynamics should closely resemble that of τ_α. Within the trap model, a measure of the α relaxation time is provided by the relaxation time τ_c defined by $C(\tau_c) = 1/e$ and measured using Eq. (8). The values of τ_c along with the values of τ_α are listed in Table I for $T = 0.6$, 0.52, and 0.48 and plotted in Fig. 7. It is clear that τ_c is much smaller than τ_α for all temperatures listed and, more importantly, τ_α increases significantly faster than τ_c. These results indicate that the trap model, as defined up to now,
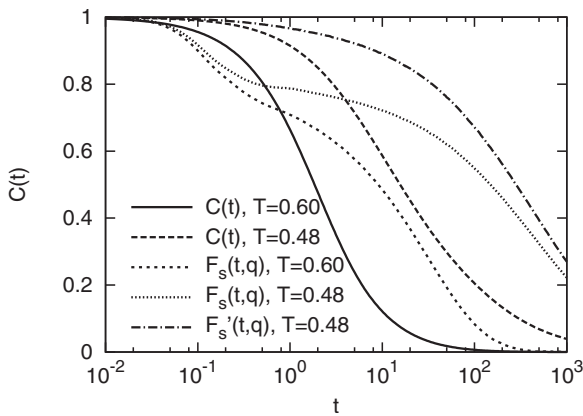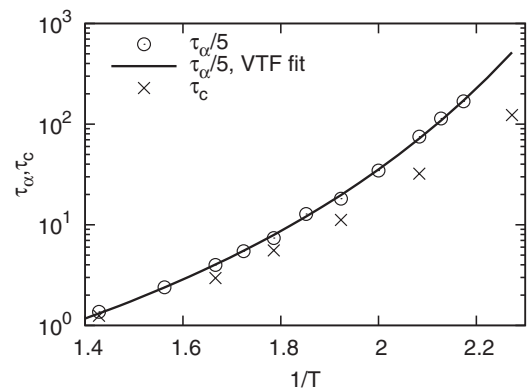
FIG. 6. Comparison of $C(t)$ obtained from the effective trap model at $T = 0.6$ and 0.48 and the incoherent-scattering function $F_s(q,t)$ measured in simulations. Also shown is $F_s'(q,t)$ the incoherent-scattering function measured from the inherent-structure coordinates. Time is measured in scaled units (cf. text).

FIG. 7. Temperature dependence of τ_α and τ_c measured in scaled units. The solid line is the fit of τ_α to the Vogel-Tamman-Fulcher form.
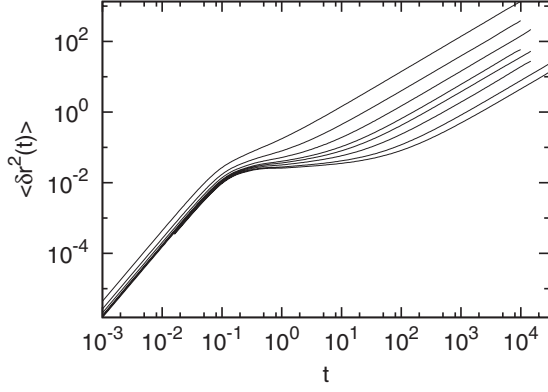
FIG. 8. MSD of type A particles plotted as a function of time t measured in scaled units. The lines correspond to $T=1.5$, 0.9, 0.7, 0.6, 0.56, 0.52, 0.48, and 0.46, top to bottom at $t \geq 1$.

does not capture all of the physical processes leading to the slow dynamics.

B. Trap model prediction of the mean-squared displacement

The mean-squared displacement (MSD) $\langle \delta r^2(t) \rangle$ of type A particles is measured directly from the simulations and, as shown in Fig. 8, there is caging. The diffusion constant can be measured by looking at the long-time behavior: $D = \langle \delta r^2(t) \rangle / 6t$ at large $\langle \delta r^2(t) \rangle$. The temperature dependence of D is shown in Fig. 10.

The MSD of particles in space can be mapped on to a random walk between metabasins [9,27]. Consider a random walk going through a sequence of N metabasins $\alpha_1 \rightarrow \alpha_2 \rightarrow \ldots \rightarrow \alpha_{N+1}$, where α_n is the label of metabasin. The metabasin coordinate sequence is labeled as $\vec{\xi}_1 \rightarrow \vec{\xi}_2 \rightarrow \ldots \rightarrow \vec{\xi}_{N+1}$. where $\vec{\xi}_n$ is a $3M$-component vector representing the coordinates of M particles in metabasin n. The diffusion constant D_{MB} of this random walk can be measured from the large N limit,

$$6MD_{MB} = \frac{\langle (\vec{\xi}_{N+1} - \vec{\xi}_1)^2 \rangle_{rw}}{N \langle \tau_n \rangle_{rw}}, \quad (9)$$

where $\langle \tau_n \rangle_{rw}$ is the average waiting time obtained by averaging over all random-walk trajectories in the metabasin space. For each metabasin α_n, the probability of being at metabasin i is proportional to $P_{i,eq}/\tau_i$. Thus, $\langle \tau_n \rangle_{rw}$ can be calculated from $\langle 1/\tau_i \rangle_{eq}$, which is an average over all metabasins weighted with equilibrium probabilities,

$$\langle \tau_n \rangle_{rw} = \frac{\sum_i \dfrac{P_{i,eq}}{\tau_i} \tau_i}{\sum_i \dfrac{P_{i,eq}}{\tau_i}} = \frac{1}{\langle 1/\tau_i \rangle_{eq}}. \quad (10)$$

Assuming that at each metabasin transition the displacement in $\vec{\xi}$ space is $\sqrt{\Delta}$, the diffusion constant D_{MB} is, therefore, $D_{MB} = (\Delta/6M)\langle 1/\tau_i \rangle_{eq}$. As shown in Fig. 10, D_{MB} rides above the D measured from the MSD of particles, again, demonstrating that the trap model picture, which ignores all

connectivity in the metabasin space, underestimates the slowing down of the dynamics.

VII. EFFECTS OF CONNECTIVITY IN METABASIN SPACE

One feature of the metabasin space that has been ignored in the trap model discussed above is that the Markovian dynamics describes a random walk on a graph with nontrivial connectivity. The calculation of the diffusion constant D_{MB} can be improved upon by incorporating aspects of the connectivity that are captured by the transition rates w_{ij}. Defining, $\delta \vec{\xi}_n = \vec{\xi}_{n+1} - \vec{\xi}_n$, the mean-squared displacement in $\vec{\xi}$ space can be written as

$$\langle (\vec{\xi}_{N+1} - \vec{\xi}_1)^2 \rangle_{rw} = \left\langle \left(\sum_{n=1}^{N} \delta \vec{\xi}_n \right)^2 \right\rangle_{rw}$$

$$= \sum_{n=1}^{N} \langle (\delta \vec{\xi}_n)^2 \rangle_{rw} + 2 \sum_{n=2}^{N} \langle \delta \vec{\xi}_{n-1} \cdot \delta \vec{\xi}_n \rangle_{rw}$$

$$+ 2 \sum_{m=2}^{N-1} \sum_{n=m+1}^{N} \langle \delta \vec{\xi}_{n-m} \cdot \delta \vec{\xi}_n \rangle_{rw}$$

$$\approx N(\Delta + 2\langle \delta \vec{\xi}_{n-1} \cdot \delta \vec{\xi}_n \rangle_{rw}). \quad (11)$$

Here, we ignored $\langle \delta \vec{\xi}_{n-m} \cdot \delta \vec{\xi}_n \rangle_{rw}$ for $m > 1$. Then the expression of D_{MB} becomes

$$6MD_{MB} \approx \langle 1/\tau_i \rangle_{eq}(\Delta + 2\langle \delta \vec{\xi}_{n-1} \cdot \delta \vec{\xi}_n \rangle_{rw}). \quad (12)$$

To calculate $\langle \delta \vec{\xi}_{n-1} \cdot \delta \vec{\xi}_n \rangle_{rw}$, one first picks the metabasin α_n at time step n to be a specific one, say i, and averages over all possible metabasins j at step $n-1$ and over all possible metabasins j' at step $n+1$ followed by averaging over all possible metabasins i at step n. For a particular $\alpha_n = i$, the probability of having a metabasin j' at $n+1$ is $w_{j'i}/\Sigma_k w_{ki} = w_{j'i}\tau_i$. Similarly, the probability of having a metabasin j at step $n-1$ must be $w_{ji}\tau_i$. Thus,

$$\langle \delta \vec{\xi}_{n-1} \cdot \delta \vec{\xi}_n \rangle_i = \langle \delta \vec{\xi}_{n-1} \rangle_i \cdot \langle \delta \vec{\xi}_n \rangle_i$$

$$= \left(\sum_j w_{ji}\tau_i \delta \vec{\xi}_{ij} \right) \cdot \left(\sum_{j'} w_{j'i}\tau_i \delta \vec{\xi}_{j'i} \right), \quad (13)$$

with $\delta \vec{\xi}_{ij} \equiv \vec{\xi}_i - \vec{\xi}_j$. Two facts should be noticed: (1) the dimension of $\vec{\xi}$, i.e., the number of independent coordinates ($d = 3M - 3 = 198$) is very high and (2) for many metabasins the connectivity is sparse, with strong connections only to one other metabasin. An example is provided by the metabasins A and B in Table II. Because of (1), any pair $\delta \vec{\xi}_{ij}$ and $\delta \vec{\xi}_{j'i}$ with $j' \neq j$ can be considered as two random vectors in a high-dimensional space and, hence, $\delta \vec{\xi}_{ij} \cdot \delta \vec{\xi}_{j'i} \approx 0$. The exception is of course when $j = j'$, i.e., when the system hops back and forth between two metabasins i and j, and $\delta \vec{\xi}_{ij} \cdot \delta \vec{\xi}_{j'i} = -(\delta \vec{\xi}_{ji})^2 = -\Delta$. So we have

$$\langle \delta \vec{\xi}_{n-1} \cdot \delta \vec{\xi}_n \rangle_i \approx -\sum_j (w_{ji}\tau_i)^2 \Delta = -p_i^2 \Delta, \quad (14)$$

where $p_i^2 \equiv \Sigma_j (w_{ji}\tau_i)^2$ is the probability of return to the previous metabasin. For those metabasins that have many neigh-

TABLE II. The branching ratio $w_{ji}\tau_i$ of four different metabasins at $T=0.52$.

i	A	B	C	D
$w_{ji}\tau_i$	0.87	0.61	0.11	0.13
	0.05	0.24	0.06	0.07
	0.02	0.06	0.05	0.05
	0.007	0.01	0.04	0.04
	0.006	0.01	0.04	0.03
	0.003	0.01	0.04	0.03
	…	…	…	…
p_i^2	0.76	0.43	0.03	0.04

bors, each with similar (and low) branching ratio $w_{j'i}\tau_i$, such as metabasins C and D in Table II, the return probability is small.

Averaging Eq. (14) over all possible metabasins i, one obtains

$$\langle \delta\vec{\xi}_{n-1} \cdot \delta\vec{\xi}_n \rangle_{rw} = \frac{\sum_i \dfrac{P_{i,eq}}{\tau_i} \langle \delta\vec{\xi}_{n-1} \cdot \delta\vec{\xi}_n \rangle_i}{\sum_i \dfrac{P_{i,eq}}{\tau_i}} \approx -\frac{\Delta\langle p_i^2/\tau_i \rangle_{eq}}{\langle 1/\tau_i \rangle_{eq}},$$

(15)

and the expression for the diffusion constant becomes

$$D_{MB} \approx \frac{\Delta}{6M}\langle (1-2p_i^2)/\tau_i \rangle_{eq}. \tag{16}$$

The branching ratios $w_{ji}\tau_i$ are measured for all the sampled metabasins and p_i^2's are calculated. As shown by the examples in Fig. 9, the return probability p_i^2 is relatively low at high temperatures. But, as the temperature decreases, p_i^2 increases significantly for some metabasins. This is because some of the transition branches are suppressed as temperature decreases. According to Eq. (16), high p_i^2 makes the diffusion constant smaller. Increasing values of p_i^2 is, therefore, another source of the slow dynamics and one that is not captured in the trap model.
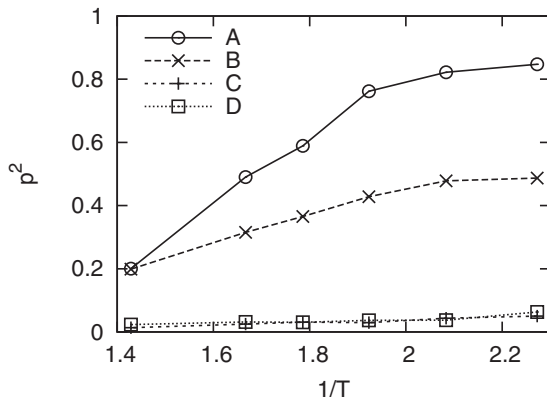

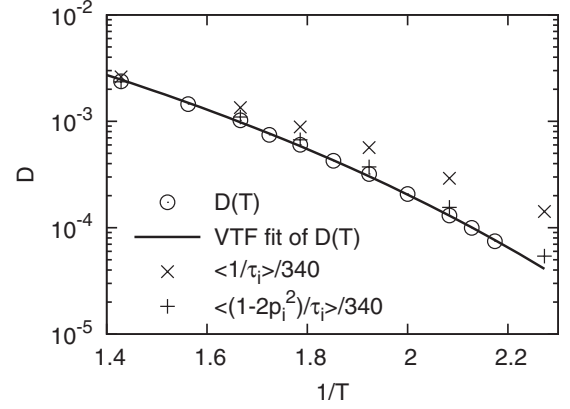FIG. 9. Comparison of $p_i^2(T)$ the return probabilities of the four metabasins listed in Table II.

FIG. 10. Comparison of the temperature dependence of the measured diffusion constant D of type A particles, with the predictions of the trap model, and the trap model modified to include a finite return probability. The relationship between the diffusion constant and τ_i in Eq. (16) has an undetermined constant, which was chosen to be 1/340 in this figure.

In Fig. 10, the prediction of Eq. (16) is compared to measured $D(T)$. It shows that incorporating the return probability p_i^2 has a significant effect on D_{MB} and improves the agreement with the measured D. In [9], Doliwa and Heuer were able to predict the diffusion constant without considering the return probability due to the fact that the metabasins were constructed from trajectories and the inherent structures that were connected by quick hops were grouped together into the same metabasin. The dynamics in the space of MB defined in this manner satisfies more stringent requirements [28], inducing $p_i^2=0$. In this work, metabasins were instead constructed from the transition branch ratio of inherent structures, without any consideration of the absolute values of the barrier heights between metabasins. The advantage of this method is that it is not based on a stochastic sampling and is more objective. The only limitations of this method are (a) that a temperature needs to be chosen *a priori* to construct the metabasins, which was chosen to be $T=0.52$ in this work, and (b) that because of the high dimensionality of the inherent-structure space simulations cannot explore the part of the space that is rarely accessed and, therefore, this method will miss some inherent structures belonging to a metabasin.

Our construction gives rise to a graph which is much more inhomogeneous and the mean-field assumption of the trap model is not a good approximation. The connectivity of the metabasin space can also be captured through the measurement of the transition rates. To emphasize, the effective dynamics in the metabasin space is certainly Markovian but the random walk lives on a graph with nontrivial connectivity.

VIII. DISCUSSION

In this work, we have presented a technique for constructing metabasins using branching ratios of transitions between inherent structures. This is different from the usual method based on molecular-dynamics trajectories [4]. The dynamics

in the space of these metabasins is Markovian and can be described as an activated process in an energy landscape. A mean-field trap model that ignores the connectivity of the metabasins, however, underestimates the slowing down of the dynamics with decreasing temperature. We show that incorporating the connectivity through a set of return probabilities leads to quantitative agreement between the predicted and measured temperature dependence of the diffusion constant. This result demonstrates that connectivity is an essential element of the effective dynamics in the metabasin space, in the temperature range analyzed ($0.48 \leq T \leq 0.7$).

All of our results regarding the structure of the metabasin space are deduced from measurement of transition rates. Since we are interested in individual metabasin transitions, it was necessary to choose a small system size in order to avoid simultaneous rearrangements of different parts of the system [4,21]. We do not study real-space dynamics and, therefore, have no information regarding the shape or size of the regions involved in a metabasin transition. Recent studies [21] of metabasin transitions in a Lennard-Jones system with a similar potential and, consisting of 150 particles, indicated that the regions involved are compact and can involve more than 60 particles. These results would imply that most of the particles in our simulation box are participating in a metabasin transition, and it is possible that the simulation box is not large enough to capture all metabasin transitions. Our simulation box with fewer than 150 particles is still larger than twice the cut-off radius for the potential used and, therefore, as in Ref. [21], the box size does not affect the interactions between particles. The transition rates measured in the simulations should, therefore, not be affected strongly by finite-size effects if the small system signals transition events that would involve much larger regions if the 67 particles were embedded within a much larger system. Simulations and single-molecule experiments [29,30] indicate that a probe molecule can be sensitive to events that involve regions much larger than the one that the probe molecule can sense directly. We are reasonably confident that the main conclusions reached in this study apply to macroscopic systems, even though our study might quantitatively underestimate some dynamical parameters. The similarity of the diffusion constant of the small system to that of larger systems [8], in the temperature regime analyzed, is a further indication that the system studied does not suffer from strong finite-size effects. We emphasize that our main focus has been to establish the nature of the effective dynamics in metabasin space (not real space) that best captures the dynamical features observed in direct simulations of our model system. In the model system, we find that the change in connectivity with decreasing temperature is an important feature that affects the slowness of the dynamics.

At temperatures higher than $\simeq 0.7$, the mean waiting time of metabasins approaches the ballistic time scale and mapping the dynamics to metabasin space loses its utility. At temperatures lower than $\simeq 0.45$, the return probabilities become so large that higher-order terms in Eq. (11) need to be included and the effective dynamics loses its simplicity. The mapping to metabasin space is, therefore, most useful in the range $0.45 < T < 0.7$ At the high end of this temperature range, the connectivity is reasonably homogeneous, and the return probabilities are low. In this regime, effective trap models capture the essential features of the slow dynamics. As the system is cooled, some of the connections are suppressed more strongly than the others. The connectivity becomes sparse, resulting in higher return probabilities, and break down of the assumption—underlying the trap model—that once the system escapes from a trap it chooses one from a fixed distribution of trap depths that does not have any connectivity information. It is clear that the difference between connections, i.e., the inhomogeneity of connectivity, causes the connectivity to be sparse at low temperatures. At the same time, we find no obvious correlation between return probability and metabasin energy and, therefore, metabasins of different energies seem to have similar connectivity environment.

Instead of metabasins, Kim and Keyes [31] considered the strong return dynamics between inherent structures of a supercooled CS_2 system and postulated that the return dynamics could be coarse grained to the motion within metabasins. In this paper, however, we showed that even after coarse-graining the strongly connected inherent structures into metabasins at a temperature in the middle of the range of interest to the slow dynamics, the connectivity between metabasins plays a significant rule, especially at low temperatures. Return dynamics appears to be less important for some small systems [32]. In general, however, if the multiple funnel landscape [13,14] is an adequate representation of the energy minima then any definition of metabasins based on a single temperature will have to include the influence of return dynamics at low enough temperatures.

[1] M. Goldstein, J. Chem. Phys. **51**, 3728 (1969).

[2] F. H. Stillinger and T. A. Weber, Science **225**, 983 (1984).

[3] F. H. Stillinger, Science **267**, 1935 (1995).

[4] S. Büchner and A. Heuer, Phys. Rev. E **60**, 6507 (1999).

[5] T. B. Schrøder and S. Sastry, J. Chem. Phys. **112**, 9834 (2000).

[6] A. Heuer, J. Phys.: Condens. Matter **20**, 373101 (2008).

[7] S. Büchner and A. Heuer, Phys. Rev. Lett. **84**, 2168 (2000).

[8] B. Doliwa and A. Heuer, Phys. Rev. Lett. **91**, 235501 (2003).

[9] B. Doliwa and A. Heuer, Phys. Rev. E **67**, 030501(R) (2003).

[10] C. Monthus and J.-P. Bouchaud, J. Phys. A **29**, 3847 (1996).

[11] R. A. Denny, D. R. Reichman, and J.-P. Bouchaud, Phys. Rev. Lett. **90**, 025503 (2003).

[12] A. Heuer, B. Doliwa, and A. Saksaengwijit, Phys. Rev. E **72**, 021503 (2005).

[13] J. Doye, M. Miller, and D. Wales, J. Chem. Phys. **111**, 8417 (1999).

[14] D. Wales, J. Doye, M. Miller, P. Mortenson, and T. Walsh, Adv. Chem. Phys. **115**, 1 (2000).

[15] W. Kob and H. C. Andersen, Phys. Rev. Lett. **73**, 1376 (1994).

[16] M. P. Allen and D. J. Tildesley, *Computer Simulation of Liquids* (Clarendon Press, New York, 1987).

[17] S. D. Stoddard and J. Ford, Phys. Rev. A **8**, 1504 (1973).

[18] Ashwin S. S and S. Sastry, J. Phys.: Condens. Matter **15**, S1253 (2003).

[19] D. Coslovich and G. Pastore, J. Chem. Phys. **127**, 124504 (2007).

[20] S. Sastry, P. G. Debenedetti, and F. H. Stillinger, Nature (London) **393**, 554 (1998).

[21] G. A. Appignanesi, J. A. Rodriguez Fris, R. A. Montani, and W. Kob, Phys. Rev. Lett. **96**, 057801 (2006).

[22] J. C. Mauro, P. K. Gupta, and R. J. Loucks, J. Chem. Phys. **126**, 184511 (2007).

[23] N. G. V. Kampen, *Stochastic Processes in Physics and Chemistry* (North-Holland, Amsterdam, 1992).

[24] F. Sciortino, W. Kob, and P. Tartaglia, Phys. Rev. Lett. **83**, 3214 (1999).

[25] J. P. Hansen and I. R. McDonald, *Theory of Simple Liquids* (Academic Press, London, 1986).

[26] G. Szamel and E. Flenner, Phys. Rev. E **73**, 011504 (2006).

[27] B. M. Schulz, S. Trimper, and M. Schulz, J. Chem. Phys. **114**, 10402 (2001).

[28] O. Rubner and A. Heuer, Phys. Rev. E **78**, 011504 (2008).

[29] R. A. L. Vallée, W. Paul, and K. Binder, J. Chem. Phys. **127**, 154903 (2007).

[30] R. A. L. Vallée, M. Van der Auweraer, W. Paul, and K. Binder, Phys. Rev. Lett. **97**, 217801 (2006).

[31] J. Kim and T. Keyes, J. Chem. Phys. **121**, 4237 (2004).

[32] T. Keyes and J. Chowdhary, Phys. Rev. E **64**, 032201 (2001).